PCCP

PAPER

View Article Online
View Journal

Cite this: DOI: 10.1039/c5cp06884c

Li_3AlSiO_5: the first aluminosilicate as a potential deep-ultraviolet nonlinear optical crystal with the quaternary diamond-like structure†

Xinglong Chen,[ab] Fangfang Zhang,*[a] Lili Liu,[ab] Bing-Hua Lei,[ab] Xiaoyu Dong,[a] Zhihua Yang,*[a] Hongyi Li[ac] and Shilie Pan*[a]

Received 10th November 2015,
Accepted 9th December 2015

DOI: 10.1039/c5cp06884c

www.rsc.org/pccp

Deep-ultraviolet (deep-UV) nonlinear optical (NLO) crystals play a crucial role in modern laser frequency conversion technology. Traditionally, the exploration of deep-UV NLO crystals is mainly focused on borates, while, the use of phosphates recently opened up a novel and promising non-boron pathway for designing new deep-UV NLO crystals. Extending this pathway to aluminosilicates led to the discovery of Li_3AlSiO_5, the first NLO crystal in this system. It crystallizes in the polar space group $Pna2_1$ (no. 33) with a quaternary diamond-like structure composed of LiO_4, AlO_4 and SiO_4 tetrahedral groups. The compound exhibits a deep-UV cut-off edge below 190 nm and is phase matchable with moderate powder second harmonic generation (SHG) intensity ($0.8KH_2PO_4$). The band gap calculated using PBE0 is 7.29 eV, indicating that the cut-off edge of the Li_3AlSiO_5 crystal can be down to 170 nm. In addition, the compound is nonhygroscopic and thermally stable up to ~1472 K. These results suggest that Li_3AlSiO_5 is a potential deep-UV NLO crystal. First-principles studies were performed to elucidate the structure–property relationship of Li_3AlSiO_5.

Introduction

Almost immediately after the invention of the laser at the beginning of the 1960s, the SHG signal in crystalline quartz was first observed by Franklin.[1] Since then crystals with NLO properties have attracted extensive commercial and academic interest.[2,3] Various high-performance NLO crystals have been obtained after continuous intensive studies over the past 50 years. The most advanced, commercially available benchmark NLO crystals include β-BaB_2O_4,[4] LiB_3O_5,[5] KH_2PO_4 (KDP),[6] $KTiOPO_4$,[7] $AgGaQ_2$ (Q = S, Se)[8] and $ZnGeP_2$,[9] which have been widely used as optoelectronic devices in the optical spectrum from the ultraviolet (UV) to infrared (IR) regions. In contrast, NLO crystals that can be practically used in the deep-UV region (below 200 nm) are relatively rare but in urgent demand.

Generally speaking, deep-UV NLO crystals must meet a series of extremely rigorous prerequisites that include not only a noncentrosymmetric crystallographic structure and phase-matching capability, but also a wide transparency window down to the deep-UV spectral region.[10] To satisfy the above-mentioned requirements, the dominant research field has been focused on the beryllium borate system. Numerous beryllium borates were reported as deep-UV NLO crystals including $KBe_2BO_3F_2$ (KBBF),[11] $Sr_2Be_2B_2O_7$,[12] $NaBeB_3O_6$,[13] $Na_2CsBe_6B_5O_{15}$,[14] $Na_2Be_4B_4O_{11}$ and $LiNa_5Be_{12}B_{12}O_{33}$,[15] *etc.* While until now, KBBF was the sole practically applicable NLO crystal working below 200 nm by direct SHG. However, KBBF is very difficult to grow to a large size because it exhibits a strong layering growth tendency and decomposes easily at a relatively low temperature.[16] Furthermore, by containing beryllium it is highly toxic and not environmentally friendly. Therefore, multiple ways have been attempted to develop new eco-friendly deep-UV NLO crystals that can overcome the demerits of KBBF. One traditional and effective way is to design and synthesize new borate crystals that preserve the structural merits of KBBF while enhancing the interlayer interactions. For example, $Li_4Sr(BO_3)_2$[17] and $Rb_3Al_3B_3O_{10}F$[18] exhibit relatively strong interlayer bonding strengths which are about 4.7 and 9.5 times as

[a] *Key Laboratory of Functional Materials and Devices for Special Environments, Xinjiang Technical Institute of Physics & Chemistry, Chinese Academy of Sciences, Xinjiang Key Laboratory of Electronic Information Materials and Devices, No. 40-1, South Beijing Road, Urumqi 830011, China. E-mail: ffzhang@ms.xjb.ac.cn, zhyang@ms.xjb.ac.cn, slpan@ms.xjb.ac.cn; Fax: +86-991-3838957; Tel: +86-991-3674558*

[b] *University of Chinese Academy of Sciences, Beijing 100049, China*

[c] *Xinjiang Products Quality Supervision & Inspection Institute of Technology, Urumqi 830011, China*

† Electronic supplementary information (ESI) available: CCDC number 1435956 for Li_3AlSiO_5; CIF file; atomic coordinates, isotropic thermal parameters and bond valence sums; selected bond lengths and angles; data of band structure calculations; optical images and theoretical morphology of Li_3AlSiO_5; thermal ellipsoid plot of the asymmetric unit; the arrangement of $[AlSiO_5]^{3-}$ slabs; UV-Vis-NIR diffuse reflectance spectrum; IR spectrum; the TG-DSC curves; calculated band structure of Li_3AlSiO_5 using DFT and PBE0. See DOI: 10.1039/c5cp06884c

large as that of KBBF, respectively. Another novel and promising way is to develop non-boron phosphates featuring PO_4 tetrahedral building blocks which are transparent down to the deep-UV region.[19] Admittedly, the SiO_4 and AlO_4 building blocks can also satisfy the deep-UV transparency requirement,[16a,18,20] thus the extension of this promising pathway is expected to obtain more candidates for deep-UV applications.

Moreover, the appropriate combination of different anionic units in the same compound has been proved to be a very effective synthetic route for developing new NLO crystals because of its significant effect of increasing the compositional flexibility of the compounds.[21,22] It is this flexibility that allows for the potential to tune the physical properties of the material for applications in nonlinear optics.[23] Guided by this strategy, our group has successfully synthesized a series of new NLO crystals with deep-UV transparency and suitable SHG responses, such as $K_3B_6O_{10}Cl$,[24] $Cs_2B_4SiO_9$,[20b] $Ba_4B_{11}O_{20}F$,[25] $Ba_4(BO_3)_3(SiO_4)\cdot Ba_3Cl$ and $Ba_4(BO_3)_3(SiO_4)\cdot Ba_3Br$.[26]

Inspired by the fruitful results achieved by the above strategies, we extended the aforementioned boron-free pathway to the aluminosilicate system. Meanwhile, we chose the alkali metal (Li) for the cations, which has no d–d electron transitions and is ideal for the transmission of the deep-UV region. Then we thoroughly investigated the Li_2O–Al_2O_3–SiO_2 system and discovered the first aluminosilicate NLO crystal Li_3AlSiO_5 through the high temperature solution method. In this paper, the synthesis, crystal structure, linear and NLO properties, and thermal behaviors as well as the theoretical studies of Li_3AlSiO_5 are comprehensively discussed.

Experimental section

Solid-state synthesis

High-purity (99.99%) Li_2CO_3, Al_2O_3, SiO_2 and NaF were used as received. The polycrystalline samples of Li_3AlSiO_5 were synthesized using the solid-state reaction method. Stoichiometric reagents Li_2CO_3 (17.734 g, 0.24 mol), Al_2O_3 (4.078 g, 0.02 mol) and SiO_2 (4.806 g, 0.04 mol) were mixed thoroughly and loaded into a corundum crucible. The mixture was preheated at 973 K for 24 h in order to decompose the carbonate. Then the samples were thoroughly ground, gradually heated to 1273 K and held at this temperature for 10 days with several intermediate grindings and mixings. The phase purity of the product was confirmed using powder X-ray diffraction (XRD) measurement (shown in Fig. 1).

Powder XRD

Powder XRD was carried out using a Bruker D2 ADVANCE X-ray diffractometer equipped with Cu Kα radiation (λ = 1.5418 Å) at room temperature. The 2θ range was 10–70° with a scan step width of 0.02° and a fixed counting time of 1 s per step.

Single-crystal growth

Single crystals of Li_3AlSiO_5 were grown from the high-temperature solution through spontaneous crystallization using NaF as the flux. The solution was prepared in a platinum crucible by melting a mixture of the polycrystalline samples of Li_3AlSiO_5 and NaF at a molar ratio of 1 : 2. Then the platinum crucible was placed in the center of a programmable temperature furnace, gradually heated to 1223 K and held at this temperature for 3 days. The temperature was decreased to 1023 K at a rate of 1 K h^{-1}. Then the platinum crucible was allowed to cool to room temperature at a rate of 10 K h^{-1}. Thus colorless and transparent crystals with sizes of submillimeter scale were obtained (Fig. S1a, ESI†). These crystals are stable in air and moisture conditions. The theoretical morphology of Li_3AlSiO_5 was simulated using the Mercury program[27] according to the Bravais–Friedel and Donnay–Harker (BFDH) theory[28] (Fig. S1b, ESI†). We can see that the as-grown crystals are in principle consistent with the theoretical morphology despite their small sizes.

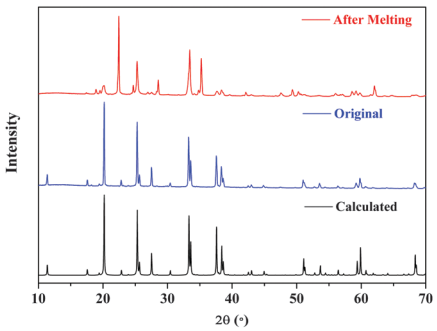

Fig. 1 Experimental and calculated XRD patterns of Li_3AlSiO_5.

X-ray crystallographic studies

A high-quality single crystal of Li_3AlSiO_5 was selected for the structure determination. It was determined using single-crystal XRD on an APEX II CCD diffractometer using graphite-monochromatic Mo Kα radiation (λ = 0.71073 Å) at 296(2) K and integrated with the SAINT program.[29] Numerical absorption corrections were carried out using the SCALE program for the area detector.[29] All calculations were performed with programs from the SHELXTL crystallographic software package.[30] All atoms were refined using full-matrix least-squares techniques. The final difference Fourier synthesis map showed the maximum and minimum peaks at 0.290 and −0.329 e $Å^{-3}$, respectively. The structure was checked with PLATON[31] and no higher symmetries were found. Crystal data and structure refinement information are given in Table 1. The final refined atomic coordinates and isotropic thermal parameters, as well as selected bond lengths and angles for Li_3AlSiO_5 are summarized in Tables S1 and S2, ESI,† respectively.

IR spectroscopy

The IR spectrum was recorded on a Shimadzu IR Affinity-1 Fourier transform IR spectrometer in the range of 400–4000 cm^{-1} with a resolution of 2 cm^{-1}. The sample was mixed thoroughly with dried KBr (4 mg of the sample and 400 mg of KBr).

UV-Vis-NIR diffuse reflectance spectrum

The optical diffuse reflectance spectrum for the Li_3AlSiO_5 polycrystalline sample was measured under a nitrogen atmosphere

Table 1 Crystal data and structure refinement information for Li_3AlSiO_5

Empirical formula	Li_3AlSiO_5
Temperature	296(2) K
Crystal system, space group	Orthorhombic, $Pna2_1$
Unit cell dimensions	a = 5.331(3) Å b = 15.551(9) Å c = 4.782(3) Å
Volume	396.4(4) Å^3
Z, calculated density	4, 2.612 g cm^{-3}
Absorption coefficient	0.715 mm^{-1}
F(000)	304
Crystal size	0.203 × 0.119 × 0.117 mm^3
Theta range for data collection	2.62 to 27.52°
Limiting indices	$-6 \le h \le 5$, $-19 \le k \le 20$, $-6 \le l \le 6$
Reflections collected/unique	2255/881 [R(int) = 0.0299]
Completeness to theta = 27.49	100.0%
Data/restraints/parameters	881/1/77
Goodness-of-fit on F^2	1.031
Final R indices [$F_o^2 > 2\sigma(F_o^2)$][a]	R_1 = 0.0287, wR_2 = 0.0667
R indices (all data)[a]	R_1 = 0.0378, wR_2 = 0.0725
Absolute structure parameter	0.12(19)
Extinction coefficient	0.014(2)
Largest diff. peak and hole	0.290 and −0.329 e Å^{-3}

[a] $R_1 = \sum\|F_o| - |F_c\|/\sum|F_o|$ and $wR_2 = [\sum w(F_o^2 - F_c^2)^2/\sum wF_o^4]^{1/2}$ for $F_o^2 > 2\sigma(F_o^2)$.

at room temperature with a Shimadzu SolidSpec-3700DUV spectrophotometer. The data were collected in the wavelength range of 190 to 2000 nm.

Second-order NLO measurements

The SHG intensities of Li_3AlSiO_5 were evaluated using the Kurtz–Perry method.[32] The measurements were carried out with a Nd:YAG pulsed solid-state laser (1064 nm, 10 kHz, 10 ns). The output light intensities emitted from the samples were collected using a photomultiplier tube. For the reason that the SHG efficiency depends strongly on particle size,[33] the polycrystalline Li_3AlSiO_5 samples were ground and sieved into the following particle size ranges: 0–20, 20–38, 38–55, 55–88, 88–105, 105–150, 150–200 μm. The microcrystalline KDP samples with the same particle size ranges served as the references.

Thermal analysis

Thermal gravimetric (TG) analysis and differential scanning calorimetry (DSC) of the Li_3AlSiO_5 were carried out on a simultaneous NETZSCH STA 449C thermal analyzer instrument. The sample was enclosed in a platinum crucible and heated with a heating rate of 10 K min^{-1} under an atmosphere of flowing nitrogen from room temperature to 1673 K.

Numerical calculation details

For the first-principles calculations, the CASTEP package,[34] a plane-wave pseudopotential method[35] based on density functional theory (DFT), was employed to analyze the electronic structure and the relationship between the optical properties and crystal structure. The structure fixed to the experimental crystallographic data was used as the original structure for the geometry optimization using the BFGS minimization technique. The converged criterion of the residual forces on the atoms, the displacements of the atoms and the energy change were less than 0.01 eV Å^{-1}, 5 × 10^{-4} Å and 5.0 × 10^{-6} eV per atom, respectively. A series of successful algorithms were executed, and finally, the Ceperley and Alder–Perdew–Zunger (CA–PZ) functional, based on the local density approximation (LDA), and the norm-conserving pseudopotential (NCP) were chosen as the exchange–correlation functional and pseudopotential. The optimized valence electronic configurations for the NCP are Li 2s^1, Al 3s^{2}3p^1, Si 3s^{2}3p^2, and O 2s^{2}2p^4 and the plane-wave cut-off energy of 1050 eV was used to ensure a small plane-wave basis set without compromising the accuracy required by our study. The Monkhorst–Pack[36] k-point meshes were set with a density of 7 × 2 × 7 with a separation of 0.03 Å^{-1} in the Brillouin zone for the electronic structures and band structures. These conditions were further applied to calculate the optical responses. In the calculation of PBE0, the Monkhorst–Pack k-point sampling 3 × 1 × 3 with a separation of 0.07 Å^{-1} was adopted. The other calculation parameters and convergent criteria were set as the default values of the CASTEP code.

The length-gauge formalism method[37] was used to estimate the SHG coefficients. At a zero frequency, the static second-order nonlinear susceptibilities can be ascribed to virtual-hole (VH) and virtual-electron (VE) processes,[38]

$$\chi^{(2)}_{\alpha\beta\gamma} = \chi^{(2)}_{\alpha\beta\gamma}(\mathrm{VE}) + \chi^{(2)}_{\alpha\beta\gamma}(\mathrm{VH}) \quad (1)$$

where $\chi^{(2)}_{\alpha\beta\gamma}(\mathrm{VE})$, $\chi^{(2)}_{\alpha\beta\gamma}(\mathrm{VH})$, and $\chi^{(2)}_{\alpha\beta\gamma}$ (two bands) are computed with the formulas as follows:

$$\chi^{(2)}_{\alpha\beta\gamma}(\mathrm{VE}) = \frac{e^3}{2\hbar m^3}\sum_{vcc'}\int\frac{d^3k}{4\pi^3}P(\alpha\beta\gamma)\mathrm{Im}\left[P^{\alpha}_{cv}P^{\beta}_{cc'}P^{\gamma}_{c'v}\right]\left(\frac{1}{\omega_{cv}{}^3\omega_{vc'}{}^2}+\frac{2}{\omega_{vc}{}^4\omega_{c'v}}\right) \quad (2)$$

$$\chi^{(2)}_{\alpha\beta\gamma}(\mathrm{VH}) = \frac{e^3}{2\hbar m^3}\sum_{vv'c}\int\frac{d^3k}{4\pi^3}P(\alpha\beta\gamma)\mathrm{Im}\left[P^{\alpha}_{vv'}P^{\beta}_{cv'}P^{\gamma}_{cv}\right]\left(\frac{1}{\omega_{cv}{}^3\omega_{v'c}{}^2}+\frac{2}{\omega_{vc}{}^4\omega_{cv'}}\right) \quad (3)$$

α, β, and γ are Cartesian components, and v and v', c and c' denote valence bands and conduction bands, respectively. $P(\alpha\beta\gamma)$, $\hbar\omega_{ij}$ and p^{α}_{ij} refer to full permutation, the band energy difference and the momentum matrix elements, respectively.

Results and discussion

Crystal structure

Li_3AlSiO_5 crystallizes in the orthorhombic crystal system with a polar space group of $Pna2_1$ (no. 33). The asymmetric unit of Li_3AlSiO_5 consists of three crystallographically independent Li atoms, one Al atom, one Si atom and five O atoms, all of which reside on general positions (Fig. S2, ESI†). All of the cations are four-coordinated forming LiO_4, AlO_4 and SiO_4 tetrahedra.

Detailed investigation of the structure has shown that the SiO_4 units are isolated from each other and each Si atom locates at the

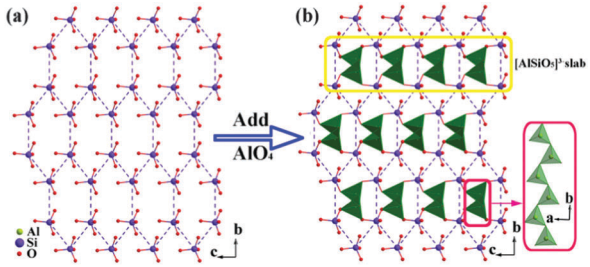

Fig. 2 (a) The arrangement of SiO_4 groups in the crystal structure of Li_3AlSiO_5, dotted lines are drawn to guide the eye; (b) formation of $[AlSiO_5]^{3-}$ anion groups.

joint of a pseudo-skeleton which exhibits 6-membered ring tunnels viewing down the *a*-axis (Fig. 2a), where the $[AlO_3]_\infty$ chains formed by corner shared AlO_4 tetrahedra reside (Fig. 2b). The connection of the SiO_4 units and the $[AlO_3]_\infty$ chains leads to the anionic $[AlSiO_5]^{3-}$ slabs as shown in Fig. 2b and Fig. S3, ESI.† In the structure, $Li(1)O_4$ tetrahedra connect with each other by vertical O atoms to form 1D $[Li(1)O_3]_\infty$ chains along the *a*-axis, and the $Li(2)O_4$ tetrahedra also make up $[Li(2)O_3]_\infty$ chains by corner-sharing along the *c*-axis; however, the $Li(3)O_4$ tetrahedra are isolated from each other (Fig. 3). The connection of these Li–O groups and the $[AlSiO_5]^{3-}$ slabs *via* the sharing of oxygen atoms results in the final structure of Li_3AlSiO_5 (Fig. 3).

In the structure of Li_3AlSiO_5, the Li–O bond lengths vary from 1.892(5) to 2.086(6) Å, the Al–O bond lengths vary from 1.749(2) to 1.776(3) Å and the Si–O bond lengths range from 1.597(2) to 1.672(2) Å. All of the bond lengths and angles for the title compound are consistent with other Li, Al or Si containing compounds reported previously.[39] The bond valence sum analyses[40] of each atom in Li_3AlSiO_5 (Li, 0.93–1.01; Al, 2.75; Si, 3.93; O, −1.91 to −2.04) indicate that the Li, Al, Si and O atoms are in oxidation states of +1, +3, +4 and −2, respectively (Table S1, ESI†). The results of the bond valence calculations further prove that the coordinations of all atoms are reasonable.

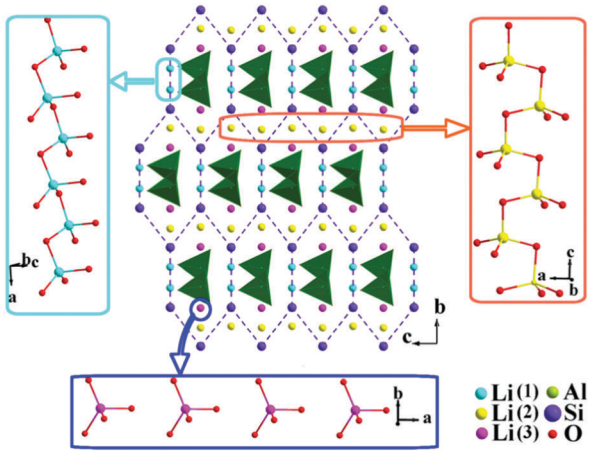

Fig. 3 Schematic diagram of the Li_3AlSiO_5 structure. (All the O atoms connected with Li and Si atoms have been omitted for clarity.)

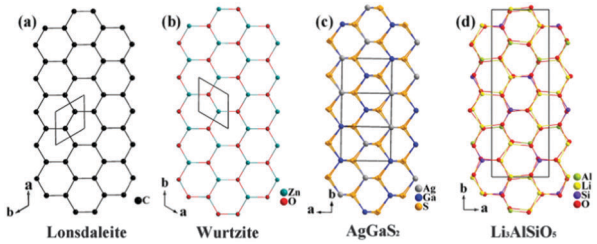

Fig. 4 The diamond-like structures from the unitary to quaternary system: (a) the structure of hexagonal diamond (lonsdaleite); (b) the structure of wurtzite (α-ZnS); (c) the structure of $AgGaS_2$; (d) the structure of Li_3AlSiO_5.

Li_3AlSiO_5 has a structure that resembles hexagonal diamond (lonsdaleite) and many famous natural and synthetic compounds that are also crystalline in diamond-like structures, for example, binary compound wurtzite (α-ZnS) and ternary compound $AgGaS_2$ (Fig. 4). In addition, numerous quaternary diamond-like semiconductors (DLSs) have been discovered (*e.g.*, Cu_2ZnSnS_4, $Cu_2ZnSnSe_4$,[41] Cu_2ZnGeS_4,[42] and Ag_2CdGeS_4[43]) and widely used in the areas of nonlinear optics,[44] thermoelectrics[45] and photovoltaics,[46] *etc.* The wide application of these quaternary compounds comes from their increased chemical and structural freedom, which make their physical properties more flexible relative to binary and ternary compounds.[47] The title compound, however, represents the quaternary diamond-like structure of an insulator. So its physical properties are worthy of study. The crystal structure has been predicted to be isostructural with Li_3AlGeO_5,[48] but the detailed information of Li_3AlSiO_5 has not been reported.

IR measurement

In order to further confirm the coordination environments of the anionic groups in the Li_3AlSiO_5 structure, IR spectroscopic measurement was carried out and the result is shown in Fig. S4, ESI.† The IR spectrum of Li_3AlSiO_5 shows high transmittance in the range of 4000–1300 cm^{-1} (2.50–7.69 μm) and displays a series of strong absorption bands with frequencies below 1300 cm^{-1}. According to previous work, the absorption bands at 1127, 1064, 1029, and 950 cm^{-1} can be assigned as the O–Si–O stretching vibrations of the SiO_4 groups. The bands at 878, 835, 457, and 441 cm^{-1} originate from the symmetric and asymmetric stretching vibrations of the Al–O bonds in the AlO_4 tetrahedra. The bands around 702 and 623 cm^{-1} are characteristic for the Si–O–Al bridges. The band around 531 cm^{-1} is assigned to the bending of the Si–O–Li bridges. The peaks observed in the IR spectrum are in agreement with other compounds containing SiO_4, AlO_4 and LiO_4 groups.[40b,49]

The UV-Vis-NIR diffuse reflectance spectrum

The UV-Vis-NIR diffuse reflectance spectra of polycrystalline Li_3AlSiO_5 are displayed in Fig. 5a and Fig. S5, ESI.† Absorption (*K*/*S*) data were calculated from the following Kubelka–Munk function: $F(R) = (1 - R)^2/2R = K/S$, where *R* is the reflectance, *K* is the absorption, and *S* is the scattering.[50] As shown in Fig. 5a and Fig. S5, ESI†, although there exists a relatively small absorption beginning from about 4.3 eV which is most probably caused by

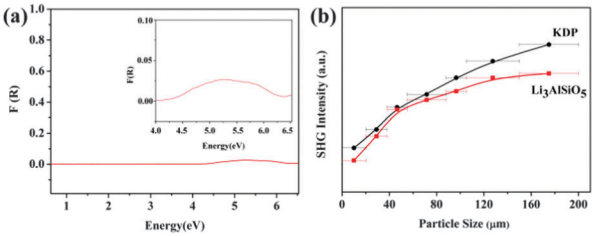

Fig. 5 (a) UV-Vis-NIR diffuse reflectance spectrum of Li_3AlSiO_5; (b) SHG intensity *vs.* particle size curve at 1064 nm for Li_3AlSiO_5, KDP samples serve as the references (the solid curves are drawn to guide the eyes and are not fits to the data).

the inescapably tiny impurity in the polycrystalline powder,[51] the sample has a large reflectance (>80%) in the range of 190–2000 nm (corresponding to 6.53–0.62 eV) and the reflectance at 190 nm is ~90%. The results indicate that the experimental band gap value of Li_3AlSiO_5 is greater than 6.53 eV; that is to say that the UV cut-off edge is below 190 nm. This value is comparable to those of Al or Si-containing deep-UV NLO crystals such as $Rb_3Al_3B_3O_{10}F$ (<200 nm),[18] $K_2Al_2B_2O_7$ (180 nm)[20a] and $Cs_2B_4SiO_9$ (<190 nm)[20b]. This suggests that the crystal may have potential applications in the deep-UV region.

NLO properties

Li_3AlSiO_5 crystallizes in a polar space group, therefore, it is expected to possess NLO properties. The curves of the SHG signal as a function of particle size are shown in Fig. 5b. It is clear that the SHG intensities become larger with the increasing particle sizes of the Li_3AlSiO_5 powders before they attain the maximization independent of the particle sizes. The result is consistent with phase-matching behavior according to the rule proposed by Kurtz and Perry.[32] It is also found that Li_3AlSiO_5 exhibits SHG responses approximately 0.8 times that of KDP in the same particle size range of 150–200 μm. Such a powder SHG efficiency is comparable to some recently reported deep-UV NLO crystals, for example β-$KBe_2B_3O_7$ (0.75KDP), γ-$KBe_2B_3O_7$ (0.68KDP), $RbBe_2B_3O_7$ (0.79KDP),[13] $Ba_3P_3O_{10}Cl$ (0.6KDP), $Ba_3P_3O_{10}Br$ (0.5KDP)[19a] and $Ba_5P_6O_{20}$ (0.8KDP).[19c]

According to the anionic group theory,[52] the SHG response of a crystal mainly comes from the contribution of anionic groups and the orientations of the anionic groups in the structure affect their total NLO contribution. Considering the arrangement of the anionic groups in Li_3AlSiO_5, it is found that all the tetrahedra groups pointing in the same direction along the *c*-axis is helpful for the crystal to generate a relatively large SHG response (see Fig. S3a, ESI†). Therefore, the alignment of the anionic tetrahedra groups in Li_3AlSiO_5 leads to its moderate SHG response.

Thermal properties

The TG-DSC curves of the Li_3AlSiO_5 crystal are shown in Fig. S6, ESI.† The TG study shows that there is no obvious weight loss in temperatures up to 1673 K. Meanwhile, two sharp endothermic peaks are observed in the DSC curve at about 1473 K and 1492 K, respectively. It is expected that Li_3AlSiO_5 is stable until heated to ~1473 K. In addition, polycrystalline Li_3AlSiO_5 was placed in a platinum crucible and heated to 1673 K, and then slowly cooled to room temperature. Powder XRD data of the solidified melt show a diffraction pattern different from that of the original Li_3AlSiO_5 powder (shown in Fig. 1). These results demonstrate that Li_3AlSiO_5 is an incongruently melting compound. Thus, large crystals of Li_3AlSiO_5 can be grown using the flux method.

Theoretical studies

In order to explore the intrinsic relationship between the electronic structure and optical properties, the first-principles studies were made. Firstly, DFT[53] was adopted to evaluate the band gap of Li_3AlSiO_5. The calculated band structure along the high symmetry points in the first brillouin zone is plotted in Fig. S7a, and the state energies along the special points are listed in Table S3a (ESI†). The results show that the highest energy of the valence band (VB) is located at the *U* point, and the lowest energy of the conduction band (CB) is located at the *G* point. Accordingly, Li_3AlSiO_5 is an indirect band gap crystal and the value of the band gap is 6.05 eV, which is less than the experimental value (>6.53 eV). The DFT usually underestimates the band gap because of the insufficient description of the eigenvalues of the electronic states. We adopted hybridization functional PBE0 to accurately predict the value of the band gap. The band structure is plotted in Fig. S7b, ESI† and the state energies along the special points are listed in Table S3b (ESI†). From the results we can see that the calculated band gap is 7.29 eV (corresponding to 170 nm). Therefore, the cut-off edge of Li_3AlSiO_5 should be down to 170 nm which is consistent with the experimental observation. It further confirms the deep-UV transparency of the Li_3AlSiO_5 crystal.

Fig. 6 displays the density of states (DOS) and partial DOS (PDOS) projected on the constitutional atoms of Li_3AlSiO_5 in the vicinity of the band gap. They can be sorted into four major distinct regions: (1) the peaks in the range of −19.0 to −15.0 eV of the VB are composed of O 2s, Li 2s, Si 3s3p and Al 3s3p states. (2) The upper part of the VB from −7.0 to 0 eV mainly arises from O 2p states, mixing with small amounts of Li 2s, Si 3s3p and Al 3s3p states. (3) The CB peaks between 6.1 to 7.5 eV are contributed by Li 2s, and Al 3s3p states, while the Li 2s state accounts for a major contribution. (4) In the range of 7.5 to 15.0 eV in the CB, O 2p, Li 2s, Si 3s3p, and Al 3s3p states are all

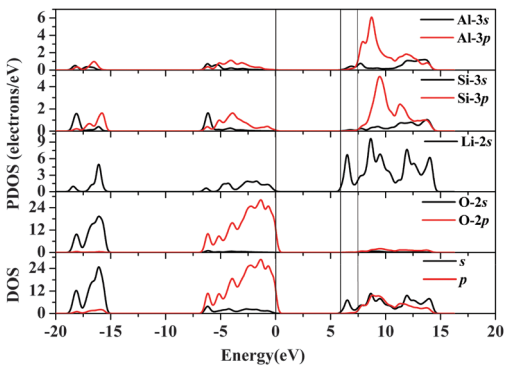

Fig. 6 The DOS and PDOS of Li_3AlSiO_5.

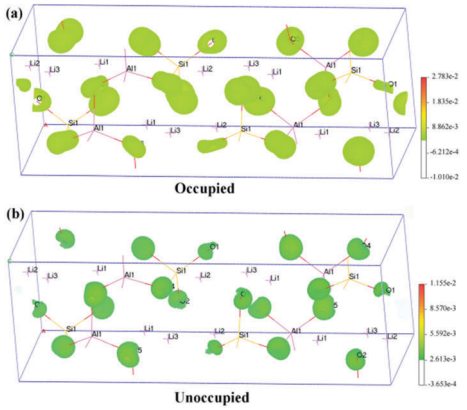

Fig. 7 The virtual-electron process of the SHG tensors for occupied states (a) and unoccupied states (b).

involved and overlap fully among them, indicating the strong interactions of Al–O, Si–O and Li–O bonds in the system. It should be emphasized that in the vicinity of the Fermi level, O 2p and Li 2s states play a dominant role implying that the interaction between Li and O may determine the band gap of Li_3AlSiO_5.

The SHG coefficients (d_{ij}) were calculated using eqn (1)–(3). The Li_3AlSiO_5 crystal allows for five nonzero SHG coefficients (d_{ij}), d_{31}, d_{32}, d_{33}, d_{24}, and d_{15} owing to its $Pna2_1$ space group. Under the restriction of Kleinman symmetry,[54] d_{31} is equal to d_{15} and d_{32} is equal to d_{24}. Therefore, there are only three independent nonzero d_{ij} coefficients, namely, d_{15}, d_{24}, and d_{33}, the values of which need to be determined. The calculated results are d_{15} = 0.091 pm V^{-1}, d_{24} = 0.247 pm V^{-1} and d_{33} = 1.41 pm V^{-1}. However, according to the symmetry of the title compound, only d_{24} is effective and it is about 0.63 times that of KDP (d_{36} = 0.39 pm V^{-1}).[55] This value is in agreement with the experimental result.

To gain further insight into the origin of the SHG effect, the SHG-density method[56] was employed to analyze the electron states response in the atoms. As for Li_3AlSiO_5, the virtual-electron makes a significant contribution (80%), therefore we will just exhibit the virtual-electron process in the SHG effect of the occupied and unoccupied states (shown in Fig. 7). As shown in Fig. 7, the 2p orbitals of the O atoms and the σ anti-bonding orbitals of AlO_4 and SiO_4 play the dominant role in the occupied and unoccupied states, respectively, while the SHG-density of AlO_4 and that of SiO_4 are almost equal. Thus we can deduce that the SHG effect of Li_3AlSiO_5 mainly originates from the cooperation of the AlO_4 and SiO_4 anionic groups. These results are consistent with the anionic group theory proposed by Chen *et al.* for the UV and deep-UV NLO crystals.[52]

Conclusions

In summary, we have successfully developed the first aluminosilicate NLO crystal Li_3AlSiO_5 using the high temperature solution method. It is eco-friendly with all the contained elements being nontoxic. Interestingly, the crystal possesses a quaternary diamond-like structure which is constructed by only tetrahedral building units with all the LiO_4, AlO_4 and SiO_4 tetrahedra pointing in the same direction, so the compound could be an ideal candidate for the study of the structure–property relationship for tetrahedron-containing compounds. Moreover, the experimental cut-off edge of Li_3AlSiO_5 is below 190 nm and further band gap calculation using PBE0 shows that the cut-off edge of Li_3AlSiO_5 can be down to 170 nm. The compound is phase matchable at the 1064 nm fundamental wavelength with a moderate powder SHG efficiency (about 0.8KDP). In addition, the crystal is nonhygroscopic and thermally stable up to 1472 K. These attributes suggest that Li_3AlSiO_5 is a potential deep-UV NLO crystal. Future efforts will be devoted to the growth of a large high-quality single crystal and the relevant physical properties studies.

Acknowledgements

The authors gratefully acknowledge the financial support of this work by the National Natural Science Foundation of China (Grant No. 21301189, 51425206, U1129301, 21461026), the Xinjiang International Science & Technology Cooperation Program (20146001), the Funds for Creative Cross & Cooperation Teams of CAS, Xinjiang Key Laboratory Foundation (Grant No. 2014KL009), the Science and Technology Project of Urumqi (Grant 51425206), and the Foundation of the Youth Innovation Promotion Association of CAS.

References

1 P. A. Franken, A. E. Hill, C. W. Peters and G. Weinreich, *Phys. Rev. Lett.*, 1961, **7**, 118–119.
2 (*a*) C. T. Chen, T. Sasaki, R. K. Li, Y. C. Wu, Z. S. Lin, Y. Mori, Z. G. Hu, J. Y. Wang, S. Uda, M. Yoshimura and Y. Kaneda, *Nonlinear Optical Borate Crystals: Principles and Applications*, Wiley-VCH, Weinheim, 2012; (*b*) T. Sasaki, Y. Mori, M. Yoshimura, Y. K. Yap and T. Kamimura, *Mater. Sci. Eng., R*, 2000, **30**, 1–54; (*c*) D. A. Keszler, *Curr. Opin. Solid State Mater. Sci.*, 1996, **1**, 204–208; (*d*) D. A. Keszler, *Curr. Opin. Solid State Mater. Sci.*, 1999, **4**, 155–162; (*e*) P. S. Halasyamani and K. R. Poeppelmeier, *Chem. Mater.*, 1998, **10**, 2753–2769.
3 (*a*) D. M. Burland, R. D. Miller and C. A. Walsh, *Chem. Rev.*, 1994, **94**, 31–75; (*b*) P. Becker, *Adv. Mater.*, 1998, **10**, 979–992; (*c*) K. M. Ok, E. O. Chi and P. S. Halasyamani, *Chem. Soc. Rev.*, 2006, **35**, 710–717; (*d*) N. Savage, *Nat. Photonics*, 2007, **1**, 83–85; (*e*) D. Cyranoaki, *Nature*, 2009, **457**, 953–955.
4 C. T. Chen, B. C. Wu, A. D. Jiang and G. M. You, *Sci. Sin., Ser. B (Engl. Ed.)*, 1985, **28**, 235–243.
5 C. T. Chen, Y. C. Wu, A. D. Jiang, B. C. Wu, G. M. You, R. K. Li and S. J. Lin, *J. Opt. Soc. Am. B*, 1989, **6**, 616–621.
6 J. J. De Yoreo, A. K. Burnham and P. K. Whitman, *Int. Mater. Rev.*, 2002, **47**, 113–152.

7 T. A. Driscoll, H. J. Hoffman, R. E. Stone and P. E. Perkins, *J. Opt. Soc. Am. B*, 1986, **3**, 683–686.
8 (*a*) A. Harasaki and K. Kato, *Jpn. J. Appl. Phys.*, 1997, **36**, 700–703; (*b*) A. H. Reshak, *J. Phys.: Condens. Matter*, 2005, **369**, 243–253.
9 G. D. Boyd, E. Buehler and F. G. Storz, *Appl. Phys. Lett.*, 1971, **18**, 301–304.
10 L. Kang, Z. S. Lin, J. G. Qin and C. T. Chen, *Sci. Rep.*, 2013, **3**, 1366.
11 (*a*) Y. N. Xia, C. T. Chen, D. Y. Tang and B. C. Wu, *Adv. Mater.*, 1995, **7**, 79–81; (*b*) C. T. Chen, G. L. Wang, X. Y. Wang and Z. Y. Xu, *Appl. Phys. B: Lasers Opt.*, 2009, **97**, 9–25.
12 C. T. Chen, Y. B. Wang, B. C. Wu, K. C. Wu, W. L. Zeng and L. H. Yu, *Nature*, 1995, **373**, 322–324.
13 S. C. Wang, N. Ye, W. Li and D. Zhao, *J. Am. Chem. Soc.*, 2010, **132**, 8779–8786.
14 S. C. Wang and N. Ye, *J. Am. Chem. Soc.*, 2011, **133**, 11458–11461.
15 H. W. Huang, L. J. Liu, S. F. Jin, W. J. Yao, Y. H. Zhang and C. T. Chen, *J. Am. Chem. Soc.*, 2013, **135**, 18319–18322.
16 (*a*) Z.-G. Hu, M. Yoshimura, Y. Mori and T. Sasaki, *J. Cryst. Growth*, 2005, **275**, 232–239; (*b*) C. T. Chen, L. Bai, Z. Z. Wang and R. K. Li, *J. Cryst. Growth*, 2006, **292**, 169–178.
17 S. G. Zhao, P. F. Gong, L. Bai, X. Xu, S. Q. Zhang, Z. H. Sun, Z. S. Lin, M. C. Hong, C. T. Chen and J. H. Luo, *Nat. Commun.*, 2014, **5**, 4019.
18 S. G. Zhao, P. F. Gong, S. Y. Luo, S. J. Liu, L. N. Li, M. A. Asghar, T. Khan, M. C. Hong, Z. S. Lin and J. H. Luo, *J. Am. Chem. Soc.*, 2015, **137**, 2207–2210.
19 (*a*) P. Yu, L.-M. Wu, L.-J. Zhou and L. Chen, *J. Am. Chem. Soc.*, 2014, **136**, 480–487; (*b*) S. G. Zhao, P. F. Gong, S. Y. Luo, L. Bai, Z. S. Lin, C. M. Ji, T. L. Chen, M. C. Hong and J. H. Luo, *J. Am. Chem. Soc.*, 2014, **136**, 8560–8563; (*c*) S. G. Zhao, P. F. Gong, S. Y. Luo, L. Bai, Z. S. Lin, Y. Y. Tang, Y. L. Zhou, M. C. Hong and J. H. Luo, *Angew. Chem.*, 2015, **127**, 4291–4295; (*d*) T. Q. Sun, P. L. Shan, H. Chen, X. W. Liu, H. D. Liu, S. L. Chen, Y. A. Cao, Y. F. Kong and J. J Xu, *CrystEngComm*, 2014, **16**, 10497–10504.
20 (*a*) Z. G. Hu, T. Higashiyama, M. Yoshimura, Y. K. Yap, Y. Mori and T. Sasaki, *Jpn. J. Appl. Phys.*, 1998, **37**, L1093–L1094; (*b*) H. P. Wu, H. W. Yu, S. L. Pan, Z. J. Huang, Z. H. Yang, X. Su and K. R. Poeppelmeier, *Angew. Chem., Int. Ed.*, 2013, **52**, 3406–3410.
21 (*a*) H. Huppertz and Z. Naturforsch, *Can. J. Res., Sect. B*, 2003, **58**, 278–290; (*b*) G. Sohr, D. M. Toebbens, J. S. auf der Gunne and H. Huppertz, *Chem. – Eur. J.*, 2014, **20**, 17059–17067; (*c*) S. L. Pan, Y. C. Wu, P. Z. Fu, G. C. Zhang, Z. H. Li, C. X. Du and C. T. Chen, *Chem. Mater.*, 2003, **15**, 2218–2221; (*d*) G. F. Wang, Y. C. Wu, P. Z. Fu, X. Y. Liang, Z. Y. Xu and C. T. Chen, *Chem. Mater.*, 2002, **14**, 2044–2047; (*e*) H. W. Yu, H. P. Wu, S. L. Pan, Z. H. Yang, X. L. Hou, X. Su, Q. Jing, K. R. Poeppelmeier and J. M. Rondinelli, *J. Am. Chem. Soc.*, 2014, **136**, 1264–1267.
22 (*a*) E. L. Belokoneva, *Crystallogr. Rev.*, 2005, **11**, 151–198; (*b*) G. Yuan and D. Xue, *Acta Crystallogr., Sect. B: Struct. Crystallogr. Cryst. Chem.*, 2007, **63**, 353–362; (*c*) G.-H. Zou, L. Huang, N. Ye, C. S. Lin, W.-D. Cheng and H. Huang, *J. Am. Chem. Soc.*, 2013, **135**, 18560–18566; (*d*) J. B. Parise and T. E. Gier, *Chem. Mater.*, 1992, **4**, 1065–1067; (*e*) Y. Z. Huang, L. M. Wu, X. T. Wu, L. H. Li, L. Chen and Y. F. Zhang, *J. Am. Chem. Soc.*, 2010, **132**, 12788–12789; (*f*) J.-L. Song, C.-L. Hu, X. Xu, F. Kong and J.-G. Mao, *Angew. Chem., Int. Ed.*, 2015, **54**, 3679–3682.
23 J. W. Lekse, M. A. Moreau, K. L. McNerny, J. Yeon, P. S. Halasyamani and J. A. Aitken, *Inorg. Chem.*, 2009, **48**, 7516–7518.
24 H. P. Wu, S. L. Pan, K. R. Poeppelmeier, H. Y. Li, D. Z. Jia, Z. H. Chen, X. Y. Fan and Y. Yang, *J. Am. Chem. Soc.*, 2011, **133**, 7786–7790.
25 H. P. Wu, H. W. Yu, Z. H. Yang, X. L. Hou, X. Su, S. L. Pan, X. Su, K. R. Poeppelmeier and J. M. Rondinelli, *J. Am. Chem. Soc.*, 2013, **135**, 4215–4218.
26 X. X. Lin, F. F. Zhang, S. L. Pan, H. W. Yu, F. Y. Zhang, X. Y. Dong, S. J. Han, L. Y. Dong, C. Y. Bai and Z. Wang, *J. Mater. Chem. C*, 2014, **2**, 4257–4264.
27 C. F. Macrae, I. J. Bruno, J. A. Chisholm, P. R. Edgington, P. McCabe, E. Pidcock, L. Rodriguez-Monge, R. Taylor, J. Streek and P. A. Wood, *J. Appl. Crystallogr.*, 2008, **41**, 466–470.
28 P. Hartman and W. G. Perdok, *Am. Mineral.*, 1937, **22**, 463–468.
29 *SAINT-Plus, version 6.02A*, Bruker Analytical X-ray Instruments, Inc., Madison, WI, 2000.
30 G. M. Sheldrick, *SHELXTL, version 6.14*, Bruker Analytical X-ray Instruments, Inc., Madison, WI, 2003.
31 A. L. Spek, *J. Appl. Crystallogr.*, 2003, **36**, 7–13.
32 S. K. Kurtz and T. T. Perry, *J. Appl. Phys.*, 1968, **39**, 3798–3813.
33 J. P. Dougherty and S. K. Kurtz, *J. Appl. Crystallogr.*, 1976, **9**, 145–158.
34 S. J. Clark, M. D. Segall, C. J. Pickard, P. J. Hasnip, M. I. J. Probert, K. Refson and M. C. Payne, *Z. Kristallogr.*, 2005, **220**, 567–570.
35 M. C. Payne, M. P. Teter, D. C. Allan, T. A. Arias and J. D. Joannopoulos, *Rev. Mod. Phys.*, 1992, **64**, 1045–1097.
36 H. J. Monkhorst and J. D. Pack, *Phys. Rev. B: Solid State*, 1976, **13**, 5188–5192.
37 C. Aversa and J. E. Sipe, *Phys. Rev. B: Condens. Matter Mater. Phys.*, 1995, **52**, 14636–14645.
38 (*a*) J. Lin, M.-H. Lee, Z.-P. Liu, C. Pickard and C. T. Chen, *Phys. Rev. B: Condens. Matter Mater. Phys.*, 1999, **60**, 13380; (*b*) B. Zhang, M.-H. Lee, Z. Yang, Q. Jing, S. Pan, M. Zhang, H. Wu, X. Su and C.-S. Li, *Appl. Phys. Lett.*, 2015, **106**, 031906.
39 (*a*) Y. Yang, S. L. Pan, X. L. Hou, C. Wang, K. R. Poeppelmeier, Z. H. Chen, H. P. Wu and Z. X. Zhou, *J. Mater. Chem.*, 2011, **21**, 2890–2894; (*b*) H. W. Yu, S. L. Pan, H. P. Wu, Z. H. Yang, L. Y. Dong, X. Su, B. B. Zhang and H. Y. Li, *Cryst. Growth Des.*, 2013, **13**, 3514–3521; (*c*) S. J. Han, S. L. Pan, Z. H. Yang, Y. Wang, B. B. Zhang, M. Zhang, Z. J. Huang, L. Y. Dong and H. W. Yu, *Z. Anorg. Allg. Chem.*, 2013, **639**, 779–783;

(*d*) F. Liebau, *Structural Chemistry of Silicates*, Springer-Verlag, New York, 1985, p. 12; (*e*) C. S. Lee, S. L. Wang, Y. H. Chen and K. H. Lii, *Inorg. Chem.*, 2009, **48**, 8357–8361; (*f*) J. D. C. Mcconnell, A. D. Vita, S. D. Kenny and V. Heine, *Phys. Chem. Miner.*, 1997, **25**, 15–23; (*g*) I. D. Brown and D. Altermatt, *Acta Crystallogr., Sect. B: Struct. Sci.*, 1985, **41**, 244–247.

40 (*a*) I. D. Brown and D. Altermatt, *Acta Crystallogr., Sect. B: Struct. Sci.*, 1985, **41**, 244–247; (*b*) N. E. Brese and M. O'keeffe, *Acta Crystallogr., Sect. B: Struct. Sci.*, 1991, **47**, 192–197.

41 C. Persson, *J. Appl. Phys.*, 2010, **107**, 053710.

42 O. V. Parasyuka, L. V. Piskacha, Y. E. Romanyukb, I. D. Olekseyuka, V. I. Zarembac and V. I. Pekhnyod, *J. Alloys Compd.*, 2005, **397**, 85–94.

43 C. D. Brunetta, W. C. Minsterman, C. H. Lake and J. A. Aitken, *J. Solid State Chem.*, 2012, **187**, 177–185.

44 (*a*) S. Levcenco, D. Dumcenco, Y. S. Huang, E. Arushanov and V. Tezlevan, *J. Alloys Compd.*, 2011, **509**, 7105–7108; (*b*) Y. Li, W. Fan, H. Sun, X. Cheng, P. Li and X. Zhao, *J. Phys.: Condens. Matter*, 2011, **23**, 225401; (*c*) J. A. Brant, D. J. Clark, Y. S. Kim, J. I. Jang, J.-H. Zhang and J. A. Aitken, *Chem. Mater.*, 2014, **26**, 3045–3048.

45 (*a*) X. Y. Shi, F. Q. Huang, M. L. Liu and L. D. Chen, *Appl. Phys. Lett.*, 2009, **94**, 122103; (*b*) M.-L. Liu, I.-W. Chen, F.-Q. Huang and L.-D. Chen, *Adv. Mater.*, 2009, **21**, 3808–3812; (*c*) C. Sevik and T. Cagin, *Appl. Phys. Lett.*, 2009, **95**, 112105; (*d*) C. Sevik and T. Cagin, *Phys. Rev. B: Condens. Matter Mater. Phys.*, 2010, **82**, 045202.

46 (*a*) Q. Guo, G. M. Ford, W. C. Yang, B. C. Walker, E. A. Stach, H. W. Hillhouse and R. Agrawal, *J. Am. Chem. Soc.*, 2010, **132**, 17384–17386; (*b*) G. M. Ford, Q. Guo, R. Agrawal and H. W. Hillhouse, *Chem. Mater.*, 2011, **23**, 2626–2629; (*c*) A. Goetzberger, C. Hebling and H. Schock, *Mater. Sci. Eng.*, 2003, **40**, 1–46.

47 S. Y. Chen, A. Walsh, Y. Luo, J.-H. Yang, X. G. Gong and S.-H. Wei, *Phys. Rev. B: Condens. Matter Mater. Phys.*, 2010, **82**, 195203.

48 J. M. S. Skakle, J. G. Fletcher, R. A. Howie, C. K. Lee and A. R. West, *J. Solid State Chem.*, 1992, **98**, 33–39.

49 (*a*) J. K. Song, D. W. Lee, Y.-H. Cho and K. M. Ok, *Bull. Korean Chem. Soc.*, 2012, **33**, 2423–2426; (*b*) M. Zhang, H. Xu, E. K. H. Salje and P. J. Heaney, *Phys. Chem. Miner.*, 2003, **30**, 457–462; (*c*) W. Lowenstein, *Am. Mineral.*, 1954, **39**, 92–96; (*d*) P. McMillan, *Am. Mineral.*, 1984, **69**, 622–644; (*e*) M. Nocun and M. Handke, *J. Mol. Struct.*, 2001, **596**, 145–149; (*f*) M. Zhang, B. Wruck, A. Graeme-Barbar, E. K. H. Salje and M. A. Carpenter, *Am. Mineral.*, 1996, **81**, 92–104.

50 (*a*) P. Kubelka and F. Z. Munk, *Tech. Phys.*, 1931, **12**, 593–601; (*b*) J. Tauc, *Mater. Res. Bull.*, 1970, **5**, 721–729.

51 (*a*) L. J. Liu, C. L. Liu, X. Y. Wang, Z. G. Hu, R. K. Li and C. T. Chen, *Solid State Sci.*, 2009, **11**, 841–844; (*b*) Z. S. Lin, L. F. Xu, L. J. Liu, J. Xu, M. H. Lee, Z. Fang and C. T. Chen, *Phys. Rev. B: Condens. Matter Mater. Phys.*, 2010, **82**, 035124; (*c*) Y. G. Wang and R. K. Li, *Opt. Mater.*, 2010, **32**, 1313–1316; (*d*) I. N. Ogorodnikov, V. A. Pustovarov, S. A. Yakovlev and L. I. Isaenko, *Opt. Mater.*, 2013, **35**, 1173–1178; (*e*) I. N. Ogorodnikov, V. A. Pustovarov, S. A. Yakovlev, L. I. Isaenko and S. A. Zhurkov, *J. Lumin.*, 2012, **132**, 1632–1638.

52 (*a*) C. T. Chen, *Sci. Sin. (Engl. Ed.)*, 1979, **22**, 756–776; (*b*) C. T. Chen and G. Z. Liu, *Annu. Rev. Mater. Sci.*, 1986, **16**, 203–243; (*c*) C. T. Chen, Y. C. Wu and R. K. Li, *Int. Rev. Phys. Chem.*, 1989, **8**, 65–91; (*d*) C. Chen, Z. Lin and Z. Wang, *Appl. Phys. B: Lasers Opt.*, 2005, **80**, 1–25.

53 J. P. Perdew and M. Levy, *Phys. Rev. Lett.*, 1983, **50**, 1884.

54 D. A. Kleinman, *Phys. Rev.*, 1962, **126**, 1977–1979.

55 R. C. Eckardt, H. Masuda, Y. X. Fan and R. L. Byer, *IEEE J. Quantum Electron.*, 1992, **28**, 2057–2074.

56 C.-H. Lo, Master degree thesis, Tamkang University, 2005.

